Journal of Southeast University (English Edition) Vol. 33, No. 1, pp. 96 - 100 Mar. 2017 ISSN 1003—7985

Effects of freeze-thaw cycles on fracture behavior of epoxy asphalt concrete

Zhang Meng Qian Zhendong

(Intelligent Transportation System Research Center, Southeast University, Nanjing 210096, China)

Abstract: According to the winter temperature of Peking, the freeze-thaw (FT) condition in laboratory was determined. Seven groups of epoxy asphalt concrete (EAC) specimen were exposed to different FT cycles. The flexural modulus and fracture energy (G_F) of EAC exposed to different FT cycles were obtained through the 3-point bending test. Meanwhile, the plane strain fracture toughness (K_{IC}) of EAC was obtained through numerical simulation. The results show that the flexural modulus of the FT conditioned EAC samples decreases with the increase of FT cycles. The FT damage of flexural modulus is 60% after 30 FT cycles. Nevertheless, with the increase of FT cycles, the G_F and K_{IC} of EAC decrease first and then increase after 15 FT cycles.

Key words: freeze-thaw cycle; epoxy asphalt concrete; flexural modulus; fracture energy; plane strain fracture toughness

DOI: 10.3969/j.issn.1003-7985.2017.01.016

The orthotropic steel bridge is widely used in the seasonal frozen area and EAC is the main pavement material for steel bridge construction. With service time passing, cracks, as well as the typical damage on the EAC pavement, will appear frequently at low temperatures. Particularly in the seasonal frozen area, the pavement of steel bridge undergoes repeating FT cycles in winter. The repeating FT cycles will not only affect the fracture behavior of EAC, but also lead to the propagation of EAC pavement cracks, which will eventually destroy the whole steel bridge pavement system.

Islam et al.[1] adopted the 4-point bending test and indirect tensile strength test to evaluate the flexural stiffness and indirect tensile strength (ITS) of FT conditioned asphalt concrete (AC). The FT cycle followed ASTM C1645 test protocol and the test results showed that the flexural stiffness of the FT conditioned samples decreased with the increase of FT cycles, whereas the ITS of AC had no significant changes. Based on 8 cycles of FT conditioning, Feng et al.[2] found that the volume and weight loss ratio of AC increased with an increase in the FT cycles. Following ASTM-C666 test protocol, rapid FT test was used to condition the AC specimens. According to the image processing technique, it was concluded that the distresses of cracks and stripping increased with each FT cycle[3]. However, FT conditioning had no negative impact on the stiffness of reclaimed asphalt pavement[4]. The Marshall stability (MS) and void ratios filled with asphalt (V_h) decreased with the increase of FT cycles, while the void volume (V_f) and void ratios inside mineral aggregate (V_{MA}) increased[5]. The FT cycle was designed by Diao et al.[6], and they concluded that the compressive strength of concrete decreased with the increasing number of freeze-thaw cycles. Jamshidi et al.[7] studied the effects of FT cycles with different freezing temperatures on cement-treated soil. The research showed that, in most cases, greater damage occurred at the end of the 12th cycle.

Most of the laboratory FT conditioning in former studies followed the ASTM test protocol, which is different from the real FT condition of seasonal frozen area. The previous researchers paid more attention to the effects of FT cycles on the pavement performance indices (e.g. MS, flexural stiffness, ITS and so on) and physical parameters (e.g. volume, weight loss ratio, V_h, V_f, V_{MA} and so on) of thermal-plastic AC, whereas they seldom concentrated on the effects of FT cycles on the fracture behavior of thermosetting EAC. The current study aims at investigating the effects of FT cycles on the fracture behavior of EAC. According to the winter temperature of Peking, the FT condition in laboratory is determined. After EAC beams were exposed to different numbers of FT cycles, the flexural modulus and G_F of EAC are studied through the 3-point bending test. Meanwhile, K_{IC} is studied through numerical simulation.

1 Laboratory Testing

1.1 Specimen fabrication

The EAC is composed of an epoxy asphalt binder, limestone filler and basalt fine graded aggregate. The epoxy asphalt binder is produced by the ChemCo System. L.P. is composed of Part A and Part B ($m_A : m_B = 1 : 5.85$). Part A is epoxy resin while Part B consists of petroleum asphalt and curing agent. The gradation is shown in Tab.1, which is the same as the gradation of EAC used in the 2nd Yangtze River Bridge pavement. The asphalt content is 6.5%.

Received 2016-06-25.

Biographies: Zhang Meng (1989—), male, graduate; Qian Zhendong (corresponding author), female, doctor, professor, qianzd@seu.edu.cn.

Foundation item: The National Natural Science Foundation of China (No. 51378122).

Citation: Zhang Meng, Qian Zhendong. Effects of freeze-thaw cycles on fracture behavior of epoxy asphalt concrete[J]. Journal of Southeast University (English Edition), 2017, 33(1): 96 - 100. DOI: 10.3969/j.issn.1003-7985.2017.01.016.

Tab. 1 Gradation of EAC

Seive size/mm		13.2	9.5	4.75	2.36	1.18	0.6	0.3	0.15	0.075
Percent passing/%	Upper limit	100	100	85	70	55	40	32	23	14
	Lower limit	100	95	65	50	39	28	21	14	7
	Designed gradation	100.0	97.1	75.0	60.0	48.0	35.0	25.0	17.4	10.5

To prepare EAC specimens, EAC slabs (30 cm × 30 cm × 5 cm) were fabricated following JTG E20—2011[8]. After 6 h of curing at 120 ℃, EAC slabs were cut into EAC specimens (20 cm × 3.5 cm × 3 cm). The EAC specimens were separated into seven groups. Each group had four specimens which were separately named *N*-1, *N*-2, *N*-3 and *N*-4 ($N = 1, 2, \ldots, 7$). *N*-1 and *N*-2 of each group are single-edge notched EAC beams (SEB) while the depth of the prefabricated crack is 1.6 cm following ASTM E399-12 test protocol[9]. *N*-3 and *N*-4 of each group are EAC beams without notch. The fabricated EAC specimens are shown in Fig. 1.

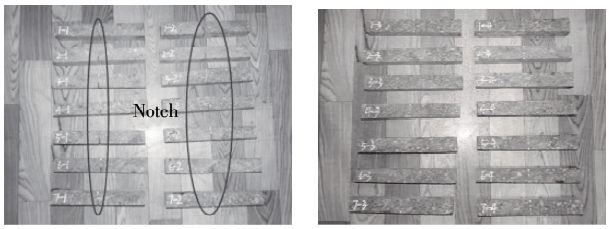

(a) (b)

Fig. 1 EAC Specimens. (a) Single-edge notched EAC beams; (b) EAC beams without notch

1.2 FT cycles in laboratory

In order to study the effects of FT cycles on the fracture behavior of EAC, the winter temperature of Peking (coordinates: 39°54′27″ N, 116°23′17″E; date: from Nov. 1, 2012 to Feb. 28, 2013) was investigated. The winter temperature of Peking was observed by the observatory of Nanjing University of Information Science & Technology for 8 times a day (observation time: 2:00, 5:00, 8:00, 11:00, 14:00, 17:00, 20:00, 23:00). According to the investigation towards the winter temperature of Peking, the average daily high temperature (T_H), average daily low temperature (T_L), average duration of daily high temperature (t_{AH}), and average duration of daily low temperature (t_{AL}) can be expressed as

$$T_L = \frac{\sum t_{LN} T_{LN}}{t_L} \tag{1}$$

$$t_{AL} = \frac{t_L}{n_{OD}} \tag{2}$$

$$T_H = \frac{\sum t_{HN} T_{HN}}{t_H} \tag{3}$$

$$t_{AH} = \frac{t_H}{n_{OD}} \tag{4}$$

where t_L represents the duration of low temperature, h; n_{OD} represents the number of observed days; t_H represents the duration of high temperature, h; t_{LN} represents the duration of low temperature at the *N*-th day, h; T_{LN} represents the average low temperature of the *N*-th day, ℃; t_{HN} represents the duration of low temperature at the *N*-th day, h; T_{HN} represents the average high temperature of the *N*-th day, ℃.

The results show that the T_L and T_H of Peking winter are −4.5 and 3.4 ℃, respectively, while the t_{AL} and t_{AH} of Peking winter are 17.8 and 6.2 h, respectively. According to the investigation of the winter temperature of Peking, the laboratory FT conditioning consists of 18 h of freezing at −5 ℃ and 6 h of soaking at 4 ℃, as shown in Fig. 2. The FT cycles for seven groups of EAC specimens are shown in Tab. 2.

(a) (b)

Fig. 2 FT conditioning of EAC specimens. (a) 18 h of freezing at −5 ℃; (b) 6 h of soaking at 4 ℃

Tab. 2 FT cycles for seven groups of EAC specimens

FT cycles	Specimen No.	FT cycles	Specimen No.
0	1-1	20	5-1
	1-2		5-2
5	2-1	25	6-1
	2-2		6-2
10	3-1	30	7-1
	3-2		7-2
15	4-1	20	5-1
	4-2		5-2

1.3 3-point bending test

The flexural modulus and K_{IC} can be determined by the 3-point bending test device[8–9]. The Universal Testing Machine (UTM) was adopted to load the EAC specimens and the loading velocity is 50 mm/min. Crack caused by transverse tensile stress is the typical damage that occurs on steel bridge EAC pavement at low temperatures. According to the investigation of the winter temperature of Peking, the minimum winter temperature of Peking is −13.8 ℃. Therefore, the temperature of the 3-point bending test in this paper is −14 ℃ which is adjusted by the thermostat. Before the 3-point bending test, all the EAC specimens were kept in the thermostat at −14 ℃ for 4 h.

2 Numerical Simulation

2.1 3-point bending test model of SEB

To study the effects of FT cycles on K_{IC} of EAC, the 3-point bending test model of SEB was established by the software ABAQUS. Three-dimensional shells were used to create SEB whose thickness was 0.03 m. Quarter-point elements[10-11] were adopted to define the crack. The middle part of the model had a dense mesh during the mesh process. Meanwhile, points B and C of the model in Fig. 3 was set to be the hinge-joints and the loading mode was set to be the displacement loading on point A, as shown in Fig. 3.

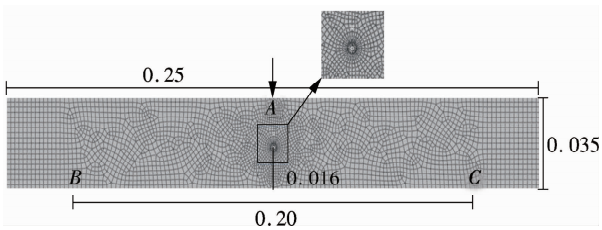

Fig. 3 3-point bending test model of EAC(unit: m)

The fracture of thermosetting EAC is a brittle fracture when the temperature is lower than 5 ℃[12]. For the simplification of modeling, EAC was assumed to be a linear elasticity material. According to the results of the 3-point bending test of EAC, the flexural moduli of EAC exposed to different FT cycles were calculated. Meanwhile, according to the test results, the average flexural modulus of each group was imported into the models, which were named Model N (N = 1, 2, …, 7), respectively, and Poisson's ratio was 0.25.

2.2 Model verification

In this paper, the mean absolute percentage error (MAPE) was adopted to represent the error between the simulation and test results. Taking Model 1 for an example, the load-displacement curve of the numerical model and laboratory test is shown in Fig. 4(a) and the absolute percentage error (APE) between the simulation and test results is shown in Fig. 4(b). Meanwhile, Fig. 5 shows the MAPE between Model N and Specimen N-1 ($MAPE_1$), the MAPE between Model N and Specimen N-2 ($MAPE_2$) and the average value of $MAPE_1$ and $MAPE_2$ ($\overline{MAPE}$).

As shown in Fig. 4, the simulation results and test results are well matched. The APE of each recorded coordinate point on the load-displacement curve is less than 1. Meanwhile, Fig. 5 shows that $\overline{MAPE}$ of each numerical model is less than 0.3. Based on the above analysis, the constructed models can be used to simulate the test.

2.3 Conditional load

Conditional load P_Q is defined as the load when $\Delta a/a$ = 2% (Δa represents the propagated depth of crack and a represents the original depth of crack). According to ASTM E399-12, for brittle material, the maximum load P_{max} is P_Q. Due to the fact that the fracture of thermosetting EAC is a brittle fracture when the temperature is lower than 5 ℃[12], P_{max} is adopted to represent P_Q of the 3-point bending test of SEB in this paper. The P_Q of each 3-point bending test of SEB is shown in Tab. 3. Meanwhile, the stress intensity factor (SIF) when the load is P_Q represents the K_{IC} of EAC.

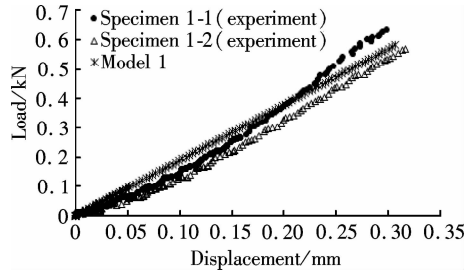

(a)

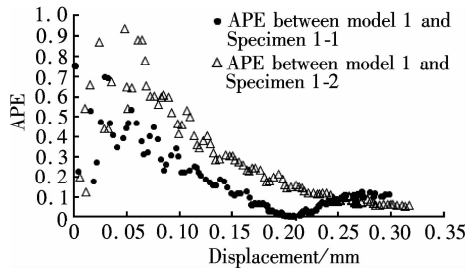

(b)

Fig. 4 Simulation results and test results. (a) Load-displacement curve of numerical model and laboratory test; (b) APE between simulation results and test results

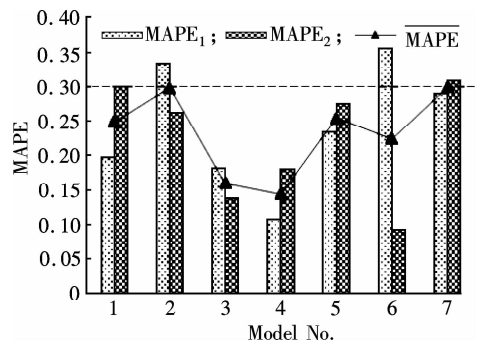

Fig. 5 MAPE between simulation results and test results of each group

Tab. 3 Conditional load of each group

Specimen No.	P_{max}/kN	P_Q/kN	Specimen No.	P_{max}/kN	P_Q/kN
1-1	0.730	0.676	5-1	0.433	0.471
1-2	0.623		5-2	0.508	
2-1	0.634	0.601	6-1	0.505	0.492
2-2	0.569		6-2	0.479	
3-1	0.491	0.485	7-1	0.622	0.581
3-2	0.480		7-2	0.541	
4-1	0.366	0.347			
4-2	0.328				

3 Results and Discussion

3.1 Effects of FT cycles on flexural modulus of EAC

The 3-point bending tests of EAC beams without notch at different FT cycles were conducted to test the flexural modulus of EAC[8]. Fig. 6 shows the decrease in flexural modulus of EAC under different FT cycles of conditioning. In the first 15 FT cycles, the flexural modulus of EAC decreases by 22% (reduced to 78%) of the original flexural modulus and the FT-induced damage on the flexural modulus of EAC is not obvious up to 15 FT cycles. The flexural modulus of EAC reduces by 60% of the original flexural modulus after 30 FT cycles and the FT-induced damage is more serious after 15 FT cycles. This signifies that FT conditioning will first cause damage to the surface binder and after a longer period of FT aging, it will cause severe damage to the in-depth binder.

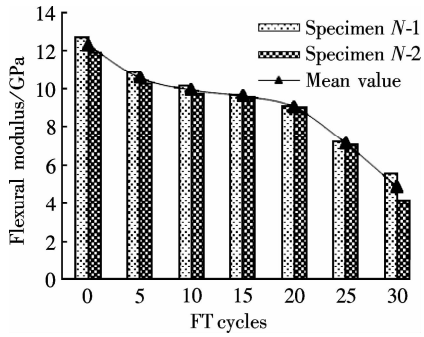

Fig. 6 Flexural modulus of EAC vs. FT cycles

3.2 Effects of FT cycles on G_F of EAC

The energy method is frequently used in fracture mechanics[13-15]. The 3-point bending test of the single-edge notched EAC beam at different cycles of FT conditioning was conducted to test the G_F of EAC. Fig. 7 shows the G_F of EAC under different FT cycles. The G_F of EAC decreases with the increase of FT cycles and after breaking a certain kind of limit, it increases with the increase of FT cycles. In the first 15 FT cycles, the G_F of EAC decreases by 56% (reduced to 44%) of the original G_F, which is caused by the decrease of the stiffness of EAC. However, after more than 15 FT cycles, the G_F of EAC increases with the increase of FT cycles, which is caused by the increase of the toughness of EAC. Moreover, the minimum G_F of EAC is observed at the 15th FT cycle.

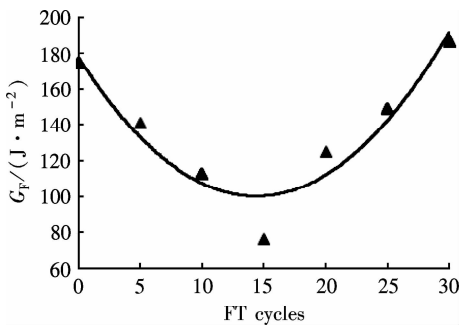

Fig. 7 G_F of EAC vs. FT cycles

3.3 Effects of FT cycles on K_{IC} of EAC

Stress intensity factor (SIF) describes the elastic stress field strength of the crack tip [10, 16]. The stress intensity factor (SIF) when the load is P_Q represents the K_{IC} of material. The closer the SIF of component with crack is to K_{IC}, the easier the crack of the component is to propagate. According to the simulation results, the K_{IC} of EAC under different FT cycles is shown in Fig. 8. The K_{IC} of EAC decreases with the increase of FT cycles and after breaking a certain kind of limit, it increases with the increase of FT cycles . In the first 15 FT cycles, the K_{IC} of EAC decreases by 37% (reduced to 63%) of the original K_{IC}, which is caused by the decrease of the stiffness of EAC. However, after more than 15 FT cycles, the K_{IC} of EAC increases with the increase of FT cycles, which is caused by the increase of the toughness of EAC. Moreover, the minimum K_{IC} of EAC is observed at the 15th FT cycle.

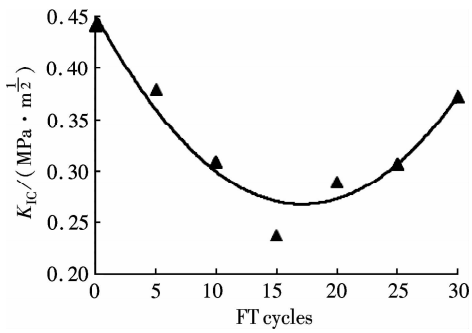

Fig. 8 K_{IC} of EAC vs. FT cycles

4 Conclusions

1) The flexural modulus of EAC decreases with the FT cycles. In the first 15 FT cycles, the flexural modulus of EAC decreases by 22% (reduced to 78%) of the original flexural modulus and the FT-induced damage on the flexural modulus of EAC is not obvious up to 15 FT cycles. The flexural modulus of EAC decreases by 60% of the original flexural modulus after 30 FT cycles and the FT-induced damage is more serious after 15 FT cycles.

2) The G_F and K_{IC} of EAC decrease with the increase of FT cycles and after breaking a certain kind of limit, they increase with the increase of FT cycles. In the first 15 FT cycles, the $G_F$and K_{IC} of EAC decreases by 56% and 37%, respectively, which is caused by the decrease of the stiffness of EAC. However, after more than 15 FT cycles, the G_F and K_{IC} of EAC increase with the increase of FT cycles, which is caused by the increase of the toughness of EAC. Moreover, the minimum G_F and K_{IC} of EAC can be observed at the 15th FT cycle.

The steel bridge deck pavement system usually includes two asphalt concrete layers and two bonding layers. How-

ever, the effects of bonding layers on the fracture behavior of EAC under different FT cycles of conditioning is not taken into account in this paper.

References

[1] Islam M R, Tarefder R A. Effects of large freeze-thaw cycles on stiffness and tensile strength of asphalt concrete [J]. *Journal of Cold Regions Engineering*, 2014, **30**(1): 06014006. DOI: 10. 1061/(asce) cr. 1943 - 5495. 0000094.

[2] Feng D, Yi J, Wang L, et al. Impact of gradation types on freeze-thaw performance of asphalt mixtures in seasonal frozen region [C]//*ICCTP Critical Issues in Transportation Systems, Planning, Development, and Management*. Harbin, China, 2009: 2336 - 2342. DOI: 10. 1061/41064 (358)328.

[3] Goh S W, You Z. Evaluation of hot-mix asphalt distress under rapid freeze-thaw cycles using image processing technique [C]//*CICTP Multimodal Transportation Systems—Convenient, Safe, Cost-Effective, Efficient*. Beijing, China, 2012: 3305 - 3315. DOI: 10. 1061/ 9780784412442. 337.

[4] Attia M, Abdelrahman M. Sensitivity of untreated reclaimed asphalt pavement to moisture, density, and freeze thaw [J]. *Journal of Materials in Civil Engineering*, 2010, **22**(12): 1260 - 1269.

[5] Özgan E, Serin S. Investigation of certain engineering characteristics of asphalt concrete exposed to freeze-thaw cycles [J]. *Cold Regions Science and Technology*, 2013, **85**: 131 - 136. DOI: 10. 1016/j. coldregions. 2012. 09. 003.

[6] Diao B, Zhang J, Ye Y, et al. Effects of freeze-thaw cycles and seawater corrosion on the behavior of reinforced air-entrained concrete beams with persistent loads [J]. *Journal of Cold Regions Engineering*, 2012, **27**(1): 44 - 53. DOI: 10. 1061/(asce) cr. 1943-5495. 0000052.

[7] Jamshidi R J, Lake C B, Barnes C L. Examining freeze/ thaw cycling and its impact on the hydraulic performance of cement-treated silty sand [J]. *Journal of Cold Regions Engineering*, 2014, **29**(3): 04014014. DOI: 10. 1061/ (asce) cr. 1943 - 5495. 0000081.

[8] Ministry of Transportation of the People's Republic of China. JTG E20—2011 Standard test method of bitumen and bituminous mixtures for highway engineering [S]. Beijing: China Communications Press, 2011. (in Chinese)

[9] American Society for Testing and Materials. ASTM E399-12 Standard test method for linear-elastic plane-strain fracture toughness KIC of metallic materials [S]. West Conshohocken, PA, USA: ASTM International, 2013.

[10] Banks-Sills L. Update: Application of the finite element method to linear elastic fracture mechanics [J]. *Applied Mechanics Reviews*, 2010, **63**(2): 020803. DOI: 10. 1115/1. 4000798.

[11] Amiri F, Anitescu C, Arroyo M, et al. XLME interpolants, a seamless bridge between XFEM and enriched meshless methods [J]. *Computational Mechanics*, 2013, **53** (1): 45 - 57. DOI: 10. 1007/s00466-013-0891-2.

[12] Qian Z D, Jing H U. Fracture properties of epoxy asphalt mixture based on extended finite element method [J]. *Journal of Central South University* (*English Edition*), 2012, **19**(11): 3335 - 3341. DOI: 10. 1007/s11771-012-1412-8.

[13] Griffith A A. The phenomena of rupture and flow in solids[J]. *Philosophical Transactions of the Royal Society A*: *Mathematical, Physical and Engineering Sciences*, 1921, **221** (582): 163 - 198. DOI: 10. 1098/rsta. 1921. 0006.

[14] Irwin G R, Kies J A. Critical energy rate analysis of fracture strength [J]. *Welding Journal*, 1954, **33**(4): 193s - 198s.

[15] Hillerborg A, Modéer M, Petersson P E. Analysis of crack formation and crack growth in concrete by means of fracture mechanics and finite elements [J]. *Cement & Concrete Research*, 1976, **6**(6): 773 - 781. DOI: 10. 1016/0008-8846(76)90007-7.

[16] Dong L T, Atluri S N. SGBEM voronoi cells (SVCs), with embedded arbitrary-shaped inclusions, voids, and/or cracks, for micromechanical modeling of heterogeneous materials[J]. *CMC*: *Computers, Materials & Continua*, 2013, **33**(2): 111 - 154.

冻融作用对环氧沥青混凝土抗裂性能的影响

张 勐 钱振东

(东南大学智能运输系统研究中心, 南京 210096)

摘要:根据北京市冬季气温调研,确定室内冻融循环试验周期,分别对7组环氧沥青混凝土试件进行不同次数的冻融循环,通过室内三点弯曲试验得到不同冻融循环次数下环氧沥青混凝土的弯曲劲度模量和断裂能,采用数值模拟方法计算不同冻融循环次数下环氧沥青混凝土的平面应变断裂韧度. 研究结果表明:环氧沥青混凝土弯曲劲度模量随冻融循环次数的增加而减小,冻融循环次数为30次时,环氧沥青混凝土弯曲劲度模量的冻融损伤量为60%;环氧沥青混凝土断裂能和平面应变断裂韧度随冻融循环次数的增加呈先减小后增大的趋势,冻融循环为15次时,环氧沥青混凝土断裂能和平面应变断裂韧度达到最小值.

关键词:冻融循环;环氧沥青混凝土;弯曲劲度模量;断裂能;平面应变断裂韧度

中图分类号:U443. 33